Light Chain of Botulinum Neurotoxin Serotype A: Structural Resolution of a Catalytic Intermediate[†,‡]

Zhuji Fu,[||] Sheng Chen,[§] Michael R. Baldwin,[§] Grant E. Boldt,[¶] Adam Crawford,[||] Kim D. Janda,[¶] Joseph T. Barbieri,[§] and Jung-Ja P. Kim*[,||]

Department of Biochemistry and Department of Microbiology and Molecular Genetics, Medical College of Wisconsin, 8701 Watertown Plank Road, Milwaukee, Wisconsin 53226, and Departments of Chemistry and Immunology, The Skaggs Institute for Chemical Biology, and Worm Institute for Research and Medicine, The Scripps Research Institute, 10550 North Torrey Pines Road, La Jolla, California 92037

Received April 22, 2006; Revised Manuscript Received May 21, 2006

ABSTRACT: Botulinum neurotoxin serotype A (BoNT/A, 1296 residues) is a zinc metalloprotease that cleaves SNAP25 to inhibit the fusion of neurotransmitter-carrying vesicles to the plasma membrane of peripheral neurons. BoNT/A is a disulfide-linked di-chain protein composed of an N-terminal, thermolysin-like metalloprotease light chain domain (LC/A, 448 residues) and a C-terminal heavy chain domain (848 residues) that can be divided into two subdomains, a translocation subdomain and a receptor binding subdomain. LC/A cleaves SNAP25 between residues Gln197−Arg198 and, unlike thermolysin, recognizes an extended region of SNAP25 for cleavage. The structure of a recombinant LC/A (1−425) treated with EDTA (No−Zn LC/A) was determined. The overall structure of No−Zn LC/A is similar to that reported for the holotoxin, except that it lacks the Zn ion, indicating that the role of Zn is catalytic not structural. In addition, structures of a noncatalytic mutant LC/A (Arg362Ala/Tyr365Phe) complexed with and without an inhibitor, ArgHX, were determined. The overall structure and the active site conformation for the mutant are the same as wild type. When the inhibitor binds to the active site, the carbonyl and N-hydroxyl groups form a bidentate ligand to the Zn ion and the arginine moiety binds to Asp369, suggesting that the inhibitor-bound structure mimics a catalytic intermediate with the Arg moiety binding at the P1′ site. Consistent with this model, mutation of Asp369 to Ala decreases the catalytic activity of LC/A by ∼600-fold, and the residual activity is not inhibited by ArgHX. These results provide new information on the reaction mechanism and insight into the development of strategies for small molecule inhibitors of BoNTs.

The botulinum neurotoxins (BoNT)[1] are zinc proteases that cleave SNARE proteins. There are seven serotypes of the botulinum toxins (A−G) which are designated by the neutralizing capacity of antitoxin sera (*1*). The BoNT serotypes A−G share ∼30−60% primary amino acid identity (*2*). The neurotoxins are synthesized as ∼150 kDa single chain proteins that are cleaved to produce disulfide linked di-chain proteins. The N-terminal ∼440 amino acids (termed the light chain, LC) include the zinc protease domain, while the C-terminal ∼800 amino acids (termed the heavy chain, HC) are organized into two domains, an internal translocation domain (HCT) and the C-terminal receptor binding domain (HCR).

Flaccid paralysis associated with botulism is due to the cleavage of SNARE proteins in peripheral neurons. A two-step serotype-specific association of BoNT with neurons has been proposed where the initial association of the HCR domain with polysialogangliosides on the cell surface precedes high-affinity binding to vesicle-associated or surface-bound proteins (*3*). In the case of BoNT/B, the toxin associates with gangliosides, which facilitate binding to synaptotagmin I and II (*4*), while BoNT/G associates with synaptotagmin I and II independent of gangliosides (*5*). BoNT/C appears to utilize glycoproteins as receptor(s) (*6*). Following receptor-mediated endocytosis, the HCT of BoNTs assists in the translocation of LC across the endocytic membrane by a pH-dependent mechanism (*7*, *8*). Each internalized LC then cleaves a specific SNARE protein, uncoupling neurotransmitter vesicle fusion capabilities. Spastic paralysis associated with tetanus toxin is due to the anterior transport of TeNT through the peripheral neuron

[†] This work was supported by a grant from the Great Lakes Regional Center of Excellence (GLRCE) from NIH-NIAID U54 AI057153 (Z.F., S.C., M.R.B., J.T.B., and J.-J.P.K.) and grants NIH-NIAID AI066507 (G.E.B., K.D.J., and J.T.B.) and NIH-NIAID BT010−04 (K.D.J.). Use of the Advanced Photon Source was supported by the United States Department of Energy, Office of Science, Office of Basic Energy Sciences, under Contract W31-109-Eng-38, and use of the BioCARS was supported by National Center for Research Resources Grant RR07707 from the National Institutes of Health.

[‡] The atomic coordinates and structure factors (PDB codes: 2G7K, 2G7P, and 2G7Q) have been deposited in the Protein Data Bank, Research Collaboratory for Structural Bioinformatics, Rutgers University, New Brunswick, NJ.

* Corresponding author. Phone, 414-456-8479; fax, 414-456-6510; e-mail, jjkim@mcw.edu.

[||] Department of Biochemistry, Medical College of Wisconsin.

[§] Department of Microbiology and Molecular Genetics, Medical College of Wisconsin.

[¶] The Scripps Research Institute.

[1] Abbreviations: BoNT/A, bolulinum neurotoxin serotype A; LC/A, BoNT/A light chain; SNAP25, synaptosomal-associated 25 kDa protein; LC/A RYM, BoNT light chain Arg362Ala/Tyr365Phe mutant; ArgHX, arginine hydroxamate.

10.1021/bi060786z CCC: $33.50
Published on Web 06/27/2006

axon where the toxin crosses the inner neuron cell junction and enters spinal inhibitory neurons where the VAMP protein is cleaved to block the release of inhibitory neurotransmitters (*9*).

BoNTs and TeNT cleave specific SNARE proteins (*3*). BoNT/A, BoNT/E, and BoNT/C cleave the membrane-bound synaptosomal-associated 25 kDa protein (SNAP25). BoNT/C also cleaves syntaxin, another membrane-bound SNARE protein. BoNT/B, BoNT/D, BoNT/F, BoNT/G, and TeNT cleave the vesicle-associated membrane protein (VAMP). Each neurotoxin cleaves a unique site on the SNARE protein with one exception; BoNT/B and TeNT cleave at the same amino acid on VAMP. Sequence recognition of the neurotoxins appears to be more complex than other zinc proteases with substrate recognition domains within and outside the active site. Both SNARE binding motifs (*10*) and an α-exosite and a *β*-exosite have been implicated in substrate recognition of SNARE proteins outside the active site (*11*). However, our understanding of the steps involved in substrate recognition is limited.

The crystal structures of BoNT/A (*12*), and BoNT/B (*13*), along with LC/A (*14*), LC/B (*15*), LC/E (*16*), LC/F (*17*), LC/G (*18*), and TeNT, (*19*) have been determined. Overall, the LC structures are similar and provide a basis for comparative functional studies. Recently, the structure of a mutated LC/A complexed with a truncated form of SNAP25 was solved (*11*). The complex structure provides insight into substrate recognition distal to the active site, but had limited information on interactions between SNAP25 and the active site presumably due to structural perturbations caused by the mutations used to inactivate catalytic activity.

Neurotoxin cleavage of SNARE proteins follows the basic molecular organization of the thermolysin family of zinc proteases. Zinc binding is coordinated by the His-Glu-X-X-His motif, a downstream glutamic acid, and a water molecule (*2, 15*). While the mechanism for peptide bond cleavage by the neurotoxins remains to be resolved, cleavage of the scissile peptide bond appears to follow a general base-catalyzed mechanism. Peptide bond cleavage is initiated by a water molecule polarized by the Glu within the Zinc binding motif (H-E-X-X-H) and Zn^{2+}, which cause a nucleophilic attack on the carbonyl carbon of the scissile bond to form an oxyanion. Peptide bond cleavage is likely achieved by a proton transfer from the attacking water mediated by the carboxyl group of a downstream Glu to form a protonated amine. In addition, a conserved Arg and Tyr (Arg362 and Tyr365 in LC/A) are proposed to stabilize the oxyanion in the transition state (*20*). Mutation of either Arg or Tyr alone lowers the velocity of cleavage with only limited effects on substrate affinity. Unexpectedly, a double mutation of Arg362 and Tyr365 to LC/A eliminated cleavage of SNAP25 to undetectable levels.

The synergistic affect of mutations to Arg and Tyr on peptide bond cleavage prompted an evaluation of how the double mutation affected the structure of the active site of LC/A. In addition, recent studies observed an inhibition of LC/A catalysis by ArgHX (Boldt,G. E. et al., *J. Comb. Chem.*, in press). To study the substrate recognition at the active site (P1 and P1′), we have determined the structure of ArgHX bound to the double mutant (Arg362Ala/Tyr365Phe), yielding insight into the catalytic mechanism of this bacterial neurotoxin.

MATERIALS AND METHODS

Expression and Purification of BoNT LC/A. Protein expression and purification were carried out as previously described (*21*). Briefly, *Escherichia coli* BL-21 RIL (DE3) cells containing the LC/A expression plasmid, pET15bLC/A (1−425), were cultured overnight on L-agar with 100 μg/mL ampicillin and 50 μg/mL chloramphenicol. Cells were inoculated into LB medium containing antibiotics and cultured at 30 °C for 2 h at 250 rpm when cells were induced with 0.75 mM IPTG, and then cultured at 250 rpm overnight at 16 °C. Cells were harvested and broken with a French Press in 40 mL of cold buffer A (20 mM Tris-HCl (pH 7.9), 1 mM DTT, 10 mM imidazole, and 0.5 M NaCl) containing EDTA-free protease inhibitor cocktail (Sigma) and 2.5 μg/mL DNAse I and 2.5 μg/mL RNAse I. The lysate was clarified by centrifugation at 20 000*g* for 20 min at 4 °C and passed through a 0.45 μm filter. The filtered lysate was applied to Ni−NTA resin (5 mL bed volume per 2 L of bacterial culture in buffer A). The column was washed with 25 mL of buffer A and eluted with 20 mM Tris-HCl, pH 7.9, containing 250 mM imidazole and 0.5 M NaCl. Peak fractions were pooled and subjected to gel-filtration on a Sephacryl S200 HR column (150 mL of resin equilibrated in 10 mM Tris-HCl (pH 7.9) and 20 mM NaCl). Peak fractions were pooled and subjected to anion exchange chromatography (10 mL of resin of DEAE-Sephacel with a 10 mM Tris-HCl (pH 7.9) with a 20−500 mM NaCl gradient). Peak fractions were pooled and dialyzed overnight into 10 mM Tris-HCl (7.6) and 20 mM NaCl with 40% glycerol (v/v). The RYM mutant was engineered using Quick Change techniques, and purified using the same procedure as the wild-type protein. Purified proteins were stored at −20 °C until ready to use.

Protease Activity of LC/A and Cleavage of SNAP25. Endopeptidase activity of the recombinant LC proteins was assayed in 40-μL of reaction mixture containing GST-SNAP25(146−205) in 20 mM K^+−HEPES, pH 7.4, and 150 mM potassium glutamate at 37 °C for 2 h. Reactions were stopped by adding SDS−PAGE sample buffer and boiling. Samples were resolved by SDS−PAGE, and the extent of cleavage was determined by visual inspection or by densitometry.

The Inhibition of LC/A and LC/A (Asp369Ala) Cleavage of SNAP25 by Arginine Hydroxamate (ArgHX). LC/A (3 nM) and LC/A(Asp369Ala) (3 μM) were incubated with the indicated concentration of ArgHX for 30 min on ice, and then 1 μg of GST-SNAP25(146−205) was added and the incubation continued for 10 min at 37 °C (total volume, 10 μL). Reactions were stopped by the addition of SDS−PAGE sample buffer and subjected to SDS−PAGE. Gels were stained, and the amount of SNAP25 cleavage was determined by densitometry.

Steady-State Kinetic Parameters for the Cleavage of SNAP25 by LC/A and LC/A(Asp369Ala). K_m and k_{cat} determinations were made for LC/A and LC/A (Asp369Ala) with SNAP25(residues 146−206). The amount of LCs was adjusted to cleave <10% substrate in various concentrations of SNAP25(146−206), between 1 and 20 μM. Reaction velocities versus substrate concentrations were fit to the Michaelis−Menten equation, and kinetic constants were derived, using the EnzFitter program (Elseiver, U.K.).

Table 1: Data Collection and Refinement Statistics

sample	LC/A-wt (No−Zn)[a]	RYM	RYM-ArgHX
resolution/highest shell (Å)	30−2.8/2.9−2.8	30.0−2.3/2.38−2.3	30.0−2.4/2.49−2.4
number of collected refs	139424	498826	490043
number of unique refs	32204/3179	57298/5677	49534/4803
completeness (%)	100/100	99.7/99.9	98.7/97.4
$I/\sigma(I)$	12.6/2.8	19.8/3.8	20.4/4.3
unit cell *a*, *b*, *c* (Å)	69.1, 110.1, 167.0	69.2,110.3, 167.1	69.3,109.9, 166.6
α, β, γ	90, 90, 90	90, 90, 90	90, 90, 90
space group	$P2_12_12_1$	$P2_12_12_1$	$P2_12_12_1$
R_{symm}	0.124/0.584	0.103/0.562	0.112/0.238
V_m (Å^3/Da)	3.18	3.19	3.18
mol. in ASU	2	2	2
	Refinement		
number of protein atoms	6470	6625	6625
water molecules		239	159
ion/number of ions		Zn^{2+}/2	Zn^{2+}/2
inhibitor atom			13
$R_{crystal}$	0.223/0.310	0.230/0.265	0.223/0.267
R_{free}	0.265/0.363	0.271/0.314	0.260/0.288
	rmsd from ideality		
bond length Å	0.008	0.007	0.007
bond angle (deg)	1.32	1.25	1.27
average *B* (Å^2)			
main chain	39.8	35.3	34.1
side chain	41.2	36.1	35.1
all atoms	40.5	35.7	34.6
water molecules	50.9	33.5	35.6
Zn ion/Inhibitor		28.8	28.2/40.3

[a] Data collected using an R-AXIS IV^{++} and all other data were collected at APS BioCARS.

Reported values are the average of at least two independent experiments performed in duplicate.

Crystallization. Crystallization experiments were performed at 21 °C using the hanging-drop vapor-diffusion method (*22*) by mixing 2 μL each of protein solution (in 30 mM HEPES, pH 7.4, and 0.1 M NaCl) and precipitating solution and equilibrating with 0.5 mL of the precipitating solution. Commercially available crystallization solutions, including Hampton Screen Kit (Hampton Research), Nextal (Nextal Biotechnology), and Wizard kits (Emerald Biostructures), were used for the initial screening of crystallization conditions. Promising conditions were then further optimized by sampling with finer screening grids.

To prevent autocatalytic cleavage during crystallization, wild-type LC/A was dialyzed against a solution containing 30 mM HEPES, pH 7.4, 0.1 M NaCl, and 1 mM EDTA and then concentrated to 15 mg/mL. For wild-type LC/A crystallization, the precipitating solution contained 0.1 M HEPES buffer, pH 7.4, 30% poly(ethylene glycol) (PEG) 1500, and 0.1 M NaCl. These crystals (hereafter referred to as No−Zn crystals) diffracted to 2.8 Å, and belong to the space group $P2_12_12_1$ with unit cell dimensions of $a = 69.2$ Å, $b = 110.4$ Å, and $c = 167.3$ Å. The asymmetric unit contained two monomers. For crystallization of the LC/A (R362A/Y365F) mutant (hereafter referred to as RYM), the protein was maintained in the same buffer as the wild-type protein, except that no EDTA treatment was included, and the precipitating solution contained 0.1 M sodium citrate, pH 5.6, 24% PEG4K, and 0.1 M NaCl. Small needle crystals appeared within a week and were isomorphous to the No−Zn crystals (space group $P2_12_12_1$ with unit cell dimensions of $a = 69.3$ Å, $b = 110.2$ Å, and $c = 167.1$ Å). As with the No−Zn crystals, the asymmetric unit contained two polypeptide chains forming a dimer, with a corresponding Mathews coefficient of $V_m = 3.2$ Å^3/Da, which corresponds to the solvent content of 61.6%. Crystals of RYM complexed with the inhibitor, ArgHX, were obtained by soaking the preformed RYM crystals in the same crystallization solution plus 4 mM inhibitor for 1 h, prior to flash-freezing in liquid nitrogen.

Data Collection. Data sets were collected at −175 °C using the mother liquor with an additional 20% glycerol as the cryoprotectant. Initial diffraction data were collected in-house using a Rigaku R-AXIS IV^{++} detector and a Micromax 007 generator equipped with an Osmic optics. Subsequently, higher resolution data sets, with the exception of the No−Zn data set, were collected using synchrotron radiation at the Advance Photon Source, BioCARS beamline 14 BM-C at the Argonne National Laboratory. DENZO and SCALEPACK implemented in the HKL2000 program package (*23*) were used to process all data. Data collection statistics are summarized in Table 1.

Structure Determination and Model Refinement. Structures were solved by the molecular replacement method with MOLREP within the CCP4 program suite (*24*) using the in-house data with the resolution range 2.0−3.0 Å. The monomer structure of LC/A (*14*) (PDB code 1E1H) was first used as the search model for the structure of RYM. The refined structure of RYM was then used as the search model for the rest of the structures. Initial models obtained from the molecular replacement solutions were further refined using the program CNS (*25*) with manual model adjustments using the program TURBO−FRODO (*26*). At later stages, water molecules were added where electron densities were higher than 3σ in the $F_o - F_c$ map. Finally, structures were refined to the highest resolution against the data collected using synchrotron radiation. The refinement statistics are given in Table 1.

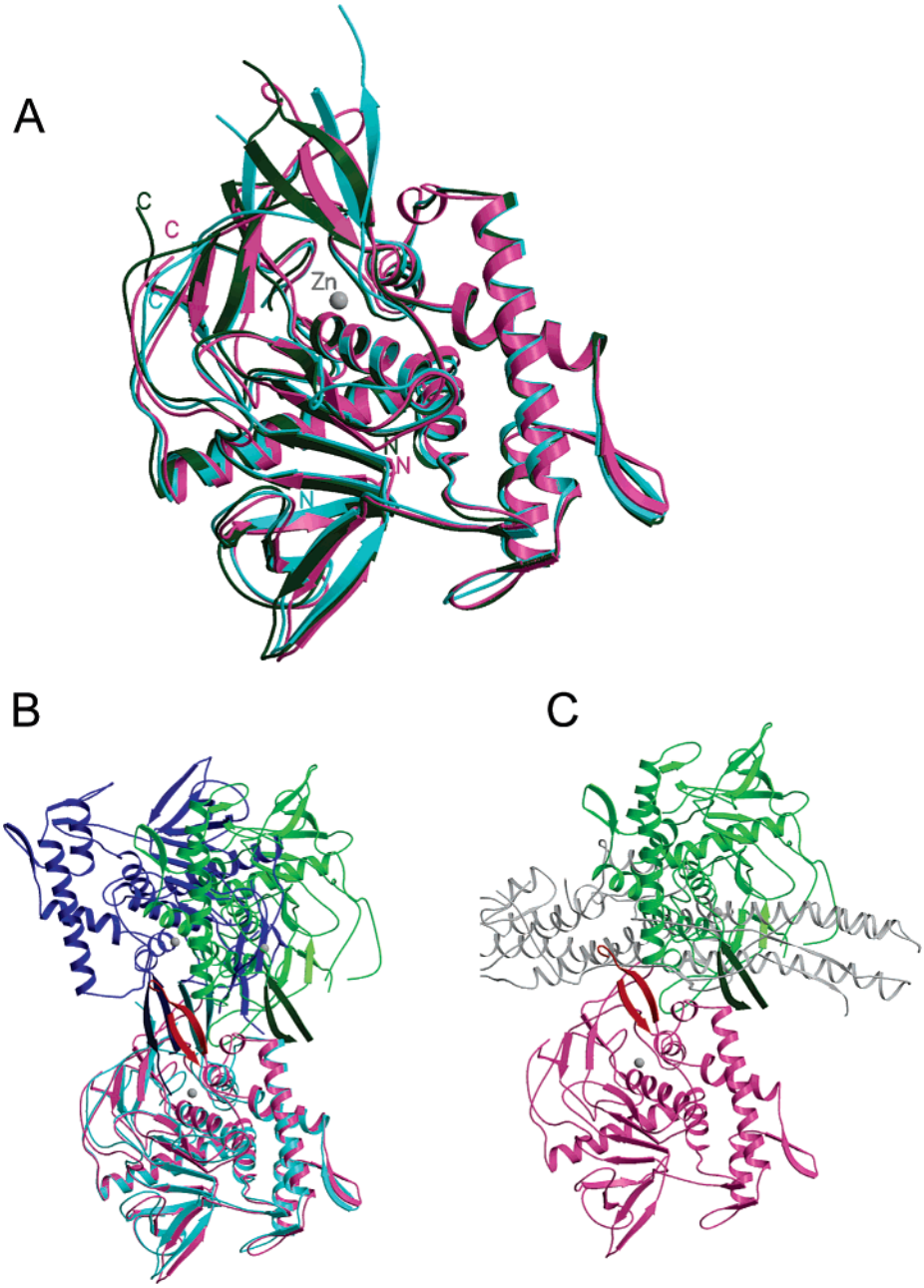

FIGURE 1: Overall polypeptide folds of the LC/A domain. (A) Superposition of LC/A structures, No−Zn LC/A (pink), the light chain portion of the holotoxin structure (dark green; PDB code, 3BTA), and the structure of autocleaved LC/A (cyan; PDB code, 1E1H). For clarity, structures of RYM and RYM/ArgHX are not included in the figure, since their rms differences from the No−Zn structure are ~0.6 Å. With the exception of the two loops (Glu196−Lys211 and Val244−Leu255; shown at the top of the figure), the structures are virtually identical. The Zn atom is shown as a gray ball. (B) Ribbon diagram of the dimeric structures of No−Zn (green and pink) and autocleaved LC/A (dark blue and cyan). The two bottom monomers are superimposed, while the top monomers are twisted by about 25° from each other, due to the loop containing Tyr249−Tyr250 of one monomer bound at the active site of the other monomer in the autocleaved LC/A structure. (C) Overlay of the dimeric No−Zn structure (pink and green) (and the autocleaved LC/A structure, which is not shown for clarity) and the translocation domains of the holotoxin structure (gray). The light chain of the holotoxin is not shown for clarity, since it superimposes well onto the pink monomer of the No−Zn structure. All figures were generated using Molscript (*44*) and Raster3D (*45*).

RESULTS AND DISCUSSION

Overall Structure. The overall polypeptide folds of each monomer are the same among the three LC/A structures (i.e., No−Zn, RYM, and RYM-ArgHX) and also are essentially the same as the Zn-containing light chain (the N-terminal 420 residues) of the holotoxin structure (*15*) and the autocleaved LC/A structure (*14*), with rms deviations ranging from 0.28 Å (between the RYM with and without ArgHX bound) to 0.85 Å (between RYM-ArgHX and the autocleaved LC/A structures (PDB code, 1E1H) for 373 residues excluding two loop areas (Glu196−Lys211 and Val244−Leu255) (Figure 1A). Since these two loops are involved in protein−protein interactions with the translocation domain in the intact holotoxin molecule, it is not surprising that these loops make intersubunit interfaces when only the light chain domain is expressed and crystallized. However, dimer formation interfaces are slightly different in two LC/A structures, No−Zn LC/A (current work) and self-cleaved

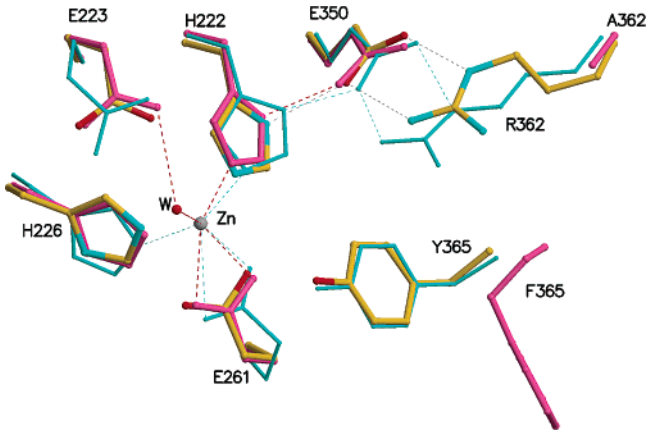

FIGURE 2: Comparisons of the active sites in various LC/A structures. The active sites of No−Zn (atom color: carbon, yellow; oxygen, red; and nitrogen, blue), RYM (pink), and the wild-type light chain structure found in the holotoxin (blue) are superimposed. The structure in the vicinity of the original Zn atom location in the No−Zn structure is essentially the same as other Zn-containing structures, including the conserved water molecule (W) that coordinates to the Zn-atom in the Zn-containing structures. Therefore, when Zn-ion is added to the EDTA-treated protein (No−Zn), the active site can be reconstituted to the active protein. In the wild-type structure (No−Zn or the intact holotoxin structure), Arg362 makes a salt bridge with Glu350, which in turn makes a hydrogen bond to His222. Tyr365 makes a hydrogen bond with Glu261, which is coordinated to the Zn atom. In the RYM structure, the phenyl ring of Phe365 is flipped away from the position of the phenol ring of Tyr365, resulting in the loss of the hydrogen bond with the carboxylate of Glu261. The Arg3626Ala mutation also removed interactions between Arg362 and Glu350.

LC/A (*14*) (Figure 1B). In the structure of the autocleaved form of LC/A, the loop containing Tyr249 of one monomer is bound to and cleaved by the active site of the other monomer of the dimeric molecule. In the No−Zn structure, the Tyr249Tyr250 portion of the loop is located on the surface of the dimeric molecule. In both cases, the dimer interface areas are similar, 2700 Å^3 for No−Zn and 2976 Å^3 for the autocleaved LC/A form. Not surprisingly, these interfaces are part of the interface between the light chain and the translocation domains in the intact toxin molecule (Figure 1C). However, whether the dimeric form of LC/A is physiologically significant is not clear at present.

Structure of the No−Zinc LC/A Active Site. The "active site" of the No−Zn structure is also the same as the Zn-containing structures, including the RYM and the intact holo-BoNT/A, except that there is no Zn atom at the center of the "active site" (Figure 2). Furthermore, there was no residual electron density at or near the site corresponding to the original Zn site, indicating that the Zn ion was completely removed from the EDTA-treated LC/A protein. In addition, no ordered water molecule was found near the Zn site. Although the side chains of Tyr249−Tyr250 are disordered, presumably due to their location at the surface of the molecule, the main chain atoms are clearly connected. Furthermore, an SDS−PAGE analysis of the crystalline protein showed that the polypeptide was intact (data not shown). This is different from the structure of the Zn-containing LC/A protein, which is cleaved at Tyr249−Tyr250 by autocatalysis (*14*). In the No−Zn structure, the two histidine residues (His222 and His226), which make coordination bonds to the Zn ion, move closer to each other only slightly (by <0.2 Å), and other active site residues are almost at the same location as in the Zn-containing RYM structure (Figure 2). Even at a relatively low resolution (2.8 Å), the No−Zn structure shows the conserved water molecule (the fourth ligand to the Zn atom), indicating that the Zn site is intact even when there is no Zn ion present. This is consistent with the fact that exogenous Zn^{2+} ion could be easily re-incorporated into the active site, restoring 50% of the catalytic activity of the apo-LC/A protein (*27*) and 100% with the apotoxin A (*28*). Furthermore, contrary to the conclusion drawn by Li and Singh (*27*), the tertiary structure of the No−Zn protein is identical to that of the Zn-containing protein. Thus, the structure of No−Zn LC/A clearly demonstrates that the role of Zn is strictly for catalytic function and is not structural.

The Active Site of the RYM Structure. Figure 2 shows an overlay of the active sites of No−Zn, RYM, and the wild-type light chain structure found in the holotoxin (*12*). The active site of RYM is the same as other LC/A structures that have been determined to date, including the structure of LC/A (Glu223Gln/Tyr365Phe) complexed with a SNAP peptide (*11*). As in other structures, the Zn ligand binding site of RYM shows a tetrahedral coordination utilizing two histidines (His222 and His226), the carboxylate of Glu261, and a water molecule, which in turn is hydrogen-bonded to Glu223. In the holotoxin structure, the absence of the fourth ligand water molecule is presumably due to the low resolution at which the structure was solved (3.3 Å). For the same reason, slightly different side chain conformations of the active site residues from those of the other two structures are most likely not significant. The Nϵ atom of His 226 is hydrogen-bonded to Glu350, which also make a salt bridge/hydrogen bond with the guanidinium group of Arg362 in the No−Zn and holotoxin structures. This salt bridge is missing in the RYM structure due to the mutation. Also absent in the RYM structure is the hydrogen bond between Tyr365 and Glu261, which is liganded to the Zn atom. Instead, Phe365 is flipped away from Glu261 and thus is far away from the Zn coordination sphere, unable to participate in the catalytic action.

On the basis of the known ability of hydroxamate derivatives to inhibit zinc metalloproteases including thermolysin (*29*), Boldt et al. observed that ArgHX inhibited the catalytic action of LC/A (*30*). A comparison of the active site structures of RYM with and without the inhibitor, L-ArgHX, is shown in Figure 3A. In the inhibitor-bound structure, the carbonyl oxygen and the N-hydroxyl group of the inhibitor are liganded to the Zn atom, and the carbonyl oxygen also makes a hydrogen bond to the carboxylate of Glu223, replacing the water molecule (fourth ligand to the Zn atom) of the apo structure. This arrangement is similar to the carboxylate of Y249 (scissile bond) observed in the structure of the autocleaved LC/A (*14*). The amide nitrogen of the hydroxamate moiety is also hydrogen-bonded to the main chain carbonyl group of Phe162. In addition, the guanidinium group makes a salt bridge with the carboxylate of Asp369. Thus, ArgHX binds at the active site and replaces the crucial catalytic water molecule, mimicking an intermediate in catalysis. In the structure of LC/A (Glu223Gln/Tyr365Phe) complexed with a truncated form of SNAP25, the P1 and P1′ residues (Gln197Arg198 of the SNAP25 peptide) are detached from the protease active site so that there are no direct interactions between the two polypeptide

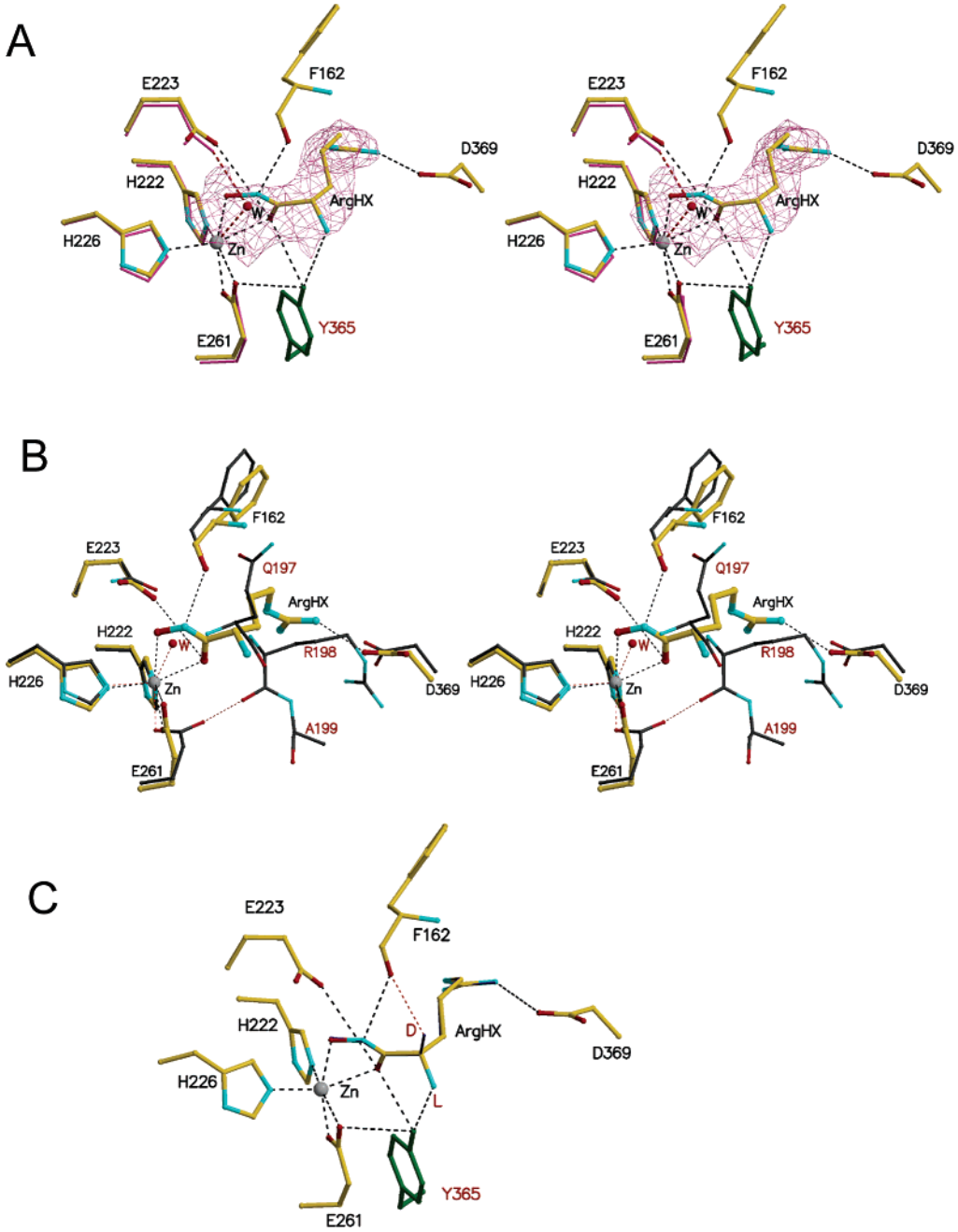

FIGURE 3: Active site structures of the Arg362Ala/Tyr365Phe mutant (RYM) alone and complexed with ArgHX. (A) Stereo diagram of an overlay of the RYM structures with (atom color) and without (pink) the inhibitor, arginine hydroxamate (ArgHX). The polypeptide structures are almost the same whether the inhibitor is bound or not. A model of L-ArgHX is fitted into the final $F_o - F_c$ omit map contoured at 3.0σ level. For clarity, coordination bonds involving the Zn atom are shown only in the inhibitor-bound structure, except that the water molecule exists only in the uncomplexed structure. The carbonyl oxygen and the N-hydroxyl group of the inhibitor make coordination bonds to the Zn atom, replacing the water molecule that is coordinated to the Zn atom in the RYM structure. The guanidinium group of the Arg side chain makes a salt bridge to Glu369, and the hydroxamate nitrogen makes a hydrogen bond with the main chain carbonyl group of Phe162. Tyr365 of the wild-type structure is shown in dark green, indicating that its hydroxyl group would make hydrogen bonds with both the amino and the carbonyl groups of the inhibitor, showing that Tyr365 is involved in proper orientation and stabilization of reaction intermediates. (B) Stereo diagram of superposition of the active site structures of RYM-ArgHX (atom color with thicker sticks) and the complex of a double mutant, Glu223Gln/Tyr365Phe, with SNAP25 (thin sticks with gray carbon atoms). Only three residues (Gln197-Arg198-Ala199) of SNAP25 are shown. Although the polypeptide direction of the SNAP25 peptide is opposite the hydroxamate inhibitor, the arginine side chain of SNAP25 can be overlaid onto the corresponding Arg group of the inhibitor, and the scissile bond carbonyl group of SNAP25 can be moved within the Zn coordination sphere near the carbonyl group of the hydroxamate inhibitor, suggesting that the binding mode of the hydroxamate inhibitor mimics an intermediate of the catalytic cycle of LC/A protease. (C) A model of D-ArgHX superimposed onto the L-form of the inhibitor. In the D-form, the hydrogen atom and the primary amino group of the L-form at the Cα atom are switched. The model indicates that both L- and D-forms can bind to the protein with equal affinities. The amino group of the L-form (labeled as L) makes a hydrogen bond to the hydroxyl group of Tyr365 (of the wild-type LC/A), while the amino group of the D-form (labeled as D) would make a hydrogen bond to the main chain carbonyl of Phe162.

chains at or near the scissile bond (*11*), presumably due to the mutations in the protease (Glu223Gln and/or Tyr365Phe).

Comparison of the active sites of the two structures (RYM/ArgHX and the SNAP25-bound LC/A structures) (Figure 3B)

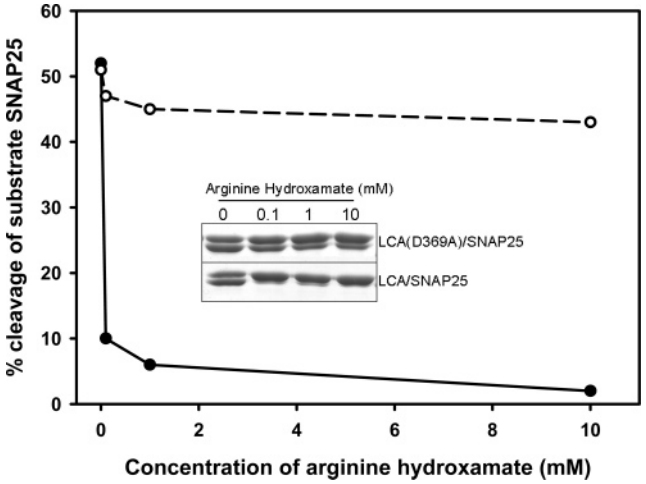

FIGURE 4: The inhibition of LC/A and LC/A(Asp369Ala) cleavage of SNAP25 by ArgHX. LC/A (●) and LC/A(Asp369Ala) (○) were incubated with the indicated concentrations of ArgHX for 30 min on ice and then incubated with 1 μg of SNAP25 for 10 min at 37 °C. The reactions were stopped and subjected to SDS−PAGE. Gels were stained, and the amount of SNAP25 cleavage was determined by densitometry. The data are from one of two independent experiments that yielded similar results; the inset shows the cleavage of SNAP25 by LCs in the presence of the indicated amount of ArgHX. The kinetic constants for SNAP25 cleavage were K_m = 16.2 ± 0.6 μM and k_{cat} = 60/s for LC/A; and K_m = 14.1 ± 1.2 μM and k_{cat} = 0.13/s for LC/A(Asp369Ala).

suggests that the SNAP peptide can be pulled into the active site such that the side chain of Arg198 can be fitted to the Arg side chain of ArgHX. Although the peptide bond direction (N→C) in the hydroxamate inhibitor is opposite to the SNAP peptide direction, the carbonyl oxygen of the scissile bond can be placed near the carbonyl group of ArgHX to coordinate to the Zn atom. This "backward" binding of an amino acid hydroxamate inhibitor in the active site has also been observed in the structure of thermolysin with L-Leu hydroxamate, in which the hydroxamate moiety complexed with the zinc and the leucyl side chain occupied the hydrophobic pocket at the P1′ site (*29*). Therefore, it is reasonable to assume that the Arg side chain of ArgHX binds to the P1′ site of RYM and the inhibitor mimics a pre-transition state intermediate of the catalytic action. While L-ArgHX inhibits LC/A activity by 75% at 50 μM concentration, at the same concentration L-glutamine hydroxamate inhibits only by 5% (*30*). The structure of RYM complexed with ArgHX explains why L-glutamine hydroxamate, which cannot make a salt bridge with Asp369, is not a good inhibitor. Furthermore, this low-affinity/inhibition effect of glutamine hydroxamate is consistent with the fact that the binding site for the arginine moiety of the inhibitor is indeed the P1′ binding site, not the P1 binding site, where Gln198 of SNAP25 would bind. To test the significance of the observed interaction between Asp369 and ArgHX, the Asp369Ala mutation was introduced into LC/A. LC/A(Asp369Ala) had a ~600-fold decrease in the rate of cleavage of SNAP25 relative to Wt-LC/A. LC/A(Asp369Ala) has a similar K_m for SNAP25 as Wt-LC/A (14.1 ± 1.2 μM versus 16.2 ± 0.6 μM), respectively, but a lower k_{cat} than Wt-LC/A (0.13/s versus 60/s), respectively. Titration experiments (Figure 4) showed that ArgHX to 10 mM did not inhibit the residual catalytic activity of LC/A(Asp369Ala) for SNAP25, while 100 μM ArgHX inhibited ~ 90% of the activity of Wt-LC/A. This is consistent with our hypothesis that the structure of LC/A in complex with ArgHX represents a catalytic intermediate.

D-ArgHX can be modeled in the active site preserving most of the interactions that are found with the L-isomer, except that the primary amino group of the D-isomer forms a hydrogen bond with the main chain carbonyl group of Phe162 (Figure 3C). This replaces the hydrogen bond between the amino group and the hydroxyl group of Tyr365 (in wild-type) in the L-isomer, indicating that the interaction strengths between the inhibitor and the polypeptide chain would be similar for the two stereoisomers. Thus, the modeled structure is consistent with the fact that the D-isomer is as good an inhibitor as the L-isomer (73% inhibition vs 75% at 50 μM inhibitor concentration). Substitution for a hydrogen atom at the amino group of ArgHX with a bulkier group ($-SO_2N(CH_3)_2$, 68% or SO_2(4-methylphenyl), 58%) does not improve the inhibitory effect (*30*). Some of the substitutions most likely cause a steric hindrance with the phenolic side chain of Tyr365 reducing binding affinities.

The Role of Arg362 and Tyr365. The active site structure of RYM is the same as that of the wild-type structure, including the location of the water molecule, the fourth ligand to the Zn. These two residues are not directly involved in the substrate binding, consistent with the results of Binz et al., showing that a single mutation of Arg362 or Tyr365 does not change the K_m values (*20*). As shown above, the role of Arg362 is to align Glu350, which in turn stabilizes His222 in the proper position to coordinate the Zn ion. Tyr365 is hydrogen-bonded to Glu261, which is a ligand to the Zn ion (Figure 2). Although conformations of Glu350 and Glu261 differ only slightly (<0.5 Å) between the structures of RYM and the LC/A of the holotoxin, the precise alignment of these residues is critical for the proper Zn coordination sphere. Therefore, Arg362 and Tyr365 are not directly involved in catalysis (i.e., not directly binding to the Zn or involved in the deprotonation/protonation reactions), but are involved in the proper alignment of the critical residues that coordinate to the Zn. In addition, if ArgHX was bound to the wild-type LC/A, Tyr365 would make hydrogen bonds with the amino group and the carboxylate of ArgHX (Figure 3A). Thus, Tyr365 might be also involved in alignment and perhaps stabilization of the transition state and/or its intermediates. Mutation of Arg362 or Tyr365 diminishes the catalytic activity to 1.2% and 2.9%, respectively, compared to the wild-type, consistent with their secondary roles in catalysis (*20*). However, when both residues are mutated, as in RYM, catalytic activity is not detectable (*20*). This is not surprising, since these two residues are involved in the alignment of two different Zn ligands (His222 via Glu350 and Glu261), and even slight misalignment of these two ligands plus destabilization of the transition state would be detrimental to the catalytic action.

CONCLUSIONS

Effective vaccines and therapies against botulism are limited. The current vaccine against botulism is a pentavalent vaccine against BoNT serotypes A−E (*31*), which is derived from chemically inactivated BoNT from *Clostridium botulinum*, but it is in limited supply. Current therapy is heptavalent immunoglobulin against BoNT serotypes A−G,

reviewed in ref *32*. Several recombinant-derived vaccine candidates are being developed that comprise the HCR domain of BoNT (*33*, *34*). Vaccination with HCR stimulates a neutralizing antibody to BoNT challenge, making this subunit a viable vaccine alternative to chemically inactivated BoNT. Recent studies showed that antibodies to the LC of BoNT stimulated a neutralizing immune response to BoNT challenge, indicating the presence of neutralizing epitopes on the LC and that a holotoxin-derived vaccine might constitute an optimal BoNT vaccine (*35*). This has prompted the development of recombinant genetically inactivated holotoxins as vaccine candidates. Currently, there are two double mutations that reduce the catalytic activity of BoNT to nondetectable levels, Glu223/Tyr365 (*11*) and Arg362/Tyr365 (20). Mutations at Arg and Tyr did not influence substrate binding affinity, but reduced the catalytic rate (*20*). The RYM structure reveals the roles of the two residues: both Arg362 and Tyr365 facilitate the proper alignment of His222 and Glu261, respectively, for the Zn coordination sphere, and Tyr is also involved in orientation and stabilization of a reaction intermediate during the catalytic action. Arg362 and Tyr365 are not present in the thermolysin active site (*36*), the prototypic zinc metalloprotease, which is consistent with Arg362 and Tyr365 being involved in the secondary role in the catalytic action of the protease. Conservation of overall structure validates BoNT/A(RYM) as a vaccine candidate. Finally, the observed structure of LC/A (RYM) in complex with ArgHX appears to represent a catalytic intermediate and identifies a new residue, Asp369, that may orient P1′ of the substrate in the active site and stabilize a reaction intermediate during catalysis.

Development of therapies against BoNT intoxication has also been limited. Two strategies that are being developed for LC inhibitors include peptides (*37*) or small molecules (*38*, *39*). Understanding how the peptides and inhibitors bind to the LCs and block catalysis will resolve the step(s) in the catalytic mechanism and provide insight into strategies to design inhibitors that block catalysis. While the structure of a noncatalytic LC/A complexed with SNAP25(146−204) (*11*) defined an α exosite and a β exosite as accessory sites for catalysis, limited information was obtained regarding the exact binding mode of the P1 and P1′ residues of SNAP25 at the active site of the protease. The structure of LC/A (RYM) in complex with ArgHX shows a completion for Zinc coordination sphere, mimicking a reaction intermediate with the arginine moiety bound at the P1′ site and providing an efficient mechanism for inhibition of catalysis. In addition, the structure defines a basis for the development of small molecule inhibitors through model-based design. The goal is to identify a small molecule that effectively inhibits multiple serotypes of BoNT catalysis without interfering with the action of host zinc metalloproteases.

While considerable effort has focused on the development of strategies for making vaccines and therapies against botulism, BoNT is the most widely utilized protein for human therapy (*40*). In addition to highly publicized cosmetic applications (*41*), BoNT is used in numerous neurological disorders from migraines to muscle trauma to physical disabilities (*42*, *43*). BoNT serotype A is the primary toxin used in these therapies, based upon the ability to produce relatively pure amounts of the holotoxin and the observed longevity of LC action in neurons. Continued comparative structure−function analysis of BoNT-LC derivatives should provide insight into mechanisms to modify BoNT to optimize therapeutic potential.

ACKNOWLEDGMENT

We acknowledge the assistance of Amanda Hill in the preparation of proteins and the staff of the BioCARS beamline at the Advanced Photon Source for support with data collection.

REFERENCES

1. Montecucco, C., and Schiavo, G. (1994) Mechanism of action of tetanus and botulinum neurotoxins, *Mol. Microbiol. 13*, 1−8.
2. Lacy, D. B., and Stevens, R. C. (1999) Sequence homology and structural analysis of the clostridial neurotoxins, *J. Mol. Biol. 291*, 1091−1104.
3. Montecucco, C., Rossetto, O., and Schiavo, G. (2004) Presynaptic receptor arrays for clostridial neurotoxins, *Trends Microbiol. 12*, 442−446.
4. Dong, M., Richards, D. A., Goodnough, M. C., Tepp, W. H., Johnson, E. A., and Chapman, E. R. (2003) Synaptotagmins I and II mediate entry of botulinum neurotoxin B into cells, *J. Cell Biol. 162*, 1293−1303.
5. Rummel, A., Karnath, T., Henke, T., Bigalke, H., and Binz, T. (2004) Synaptotagmins I and II act as nerve cell receptors for botulinum neurotoxin G, *J. Biol. Chem. 279*, 30865−30870.
6. Nishikawa, A., Uotsu, N., Arimitsu, H., Lee, J. C., Miura, Y., Fujinaga, Y., Nakada, H., Watanabe, T., Ohyama, T., Sakano, Y., and Oguma, K. (2004) The receptor and transporter for internalization of *Clostridium botulinum* type C progenitor toxin into HT-29 cells, *Biochem. Biophys. Res. Commun. 319*, 327−333.
7. Finkelstein, A. (1990) Channels formed in phospholipid bilayer membranes by diphtheria, tetanus, botulinum and anthrax toxin, *J. Physiol. (Paris) 84*, 188−190.
8. Montecucco, C., Schiavo, G., Gao, Z., Bauerlein, E., Boquet, P., and DasGupta, B. R. (1988) Interaction of botulinum and tetanus toxins with the lipid bilayer surface, *Biochem. J. 251*, 379−383.
9. Lalli, G., Gschmeissner, S., and Schiavo, G. (2003) Myosin Va and microtubule-based motors are required for fast axonal retrograde transport of tetanus toxin in motor neurons, *J. Cell Sci. 116*, 4639−4650.
10. Washbourne, P., Pellizzari, R., Baldini, G., Wilson, M. C., and Montecucco, C. (1997) Botulinum neurotoxin types A and E require the SNARE motif in SNAP-25 for proteolysis, *FEBS Lett. 418*, 1−5.
11. Breidenbach, M. A., and Brunger, A. T. (2004) Substrate recognition strategy for botulinum neurotoxin serotype A, *Nature 432*, 925−929.
12. Lacy, D. B., Tepp, W., Cohen, A. C., DasGupta, B. R., and Stevens, R. C. (1998) Crystal structure of botulinum neurotoxin type A and implications for toxicity, *Nat. Struct. Biol. 5*, 898−902.
13. Swaminathan, S., and Eswaramoorthy, S. (2000) Structural analysis of the catalytic and binding sites of *Clostridium botulinum* neurotoxin B, *Nat. Struct. Biol. 7*, 693−699.
14. Segelke, B., Knapp, M., Kadkhodayan, S., Balhorn, R., and Rupp, B. (2004) Crystal structure of *Clostridium botulinum* neurotoxin protease in a product-bound state: evidence for noncanonical zinc protease activity, *Proc. Natl. Acad. Sci. U.S.A. 101*, 6888−6893.
15. Hanson, M. A., and Stevens, R. C. (2000) Cocrystal structure of synaptobrevin-II bound to botulinum neurotoxin type B at 2.0 Å resolution, *Nat. Struct. Biol. 7*, 687−692.
16. Agarwal, R., Eswaramoorthy, S., Kumaran, D., Binz, T., and Swaminathan, S. (2004) Structural analysis of botulinum neurotoxin type E catalytic domain and its mutant Glu212 → Gln reveals the pivotal role of the Glu212 carboxylate in the catalytic pathway, *Biochemistry 43*, 6637−6644.
17. Agarwal, R., Binz, T., and Swaminathan, S. (2005) Structural analysis of botulinum neurotoxin serotype F light chain: implications on substrate binding and inhibitor design, *Biochemistry 44*, 11758−11765.
18. Arndt, J. W., Yu, W., Bi, F., and Stevens, R. C. (2005) Crystal structure of botulinum neurotoxin type G light chain: serotype divergence in substrate recognition, *Biochemistry 44*, 9574−9580.

19. Breidenbach, M. A., and Brunger, A. T. (2005) 2.3 A crystal structure of tetanus neurotoxin light chain, *Biochemistry 44*, 7450−7457.
20. Binz, T., Bade, S., Rummel, A., Kollewe, A., and Alves, J. (2002) Arg(362) and Tyr(365) of the botulinum neurotoxin type a light chain are involved in transition state stabilization, *Biochemistry 41*, 1717−1723.
21. Baldwin, M. R., Bradshaw, M., Johnson, E. A., and Barbieri, J. T. (2004) The C-terminus of botulinum neurotoxin type A light chain contributes to solubility, catalysis, and stability, *Protein Expression Purif. 37*, 187−195.
22. McPherson, A. (1999) *Crystallization of Biological Macromolecules*, Cold Spring Harbor Laboratory Press, Cold Spring Harbor, New York.
23. Otwinowski, Z., and Minor, W. (1997) Processing of X-ray diffraction data collected in oscillation mode, *Methods Enzymol. 276*, 307−326.
24. Collaborative Computational Project, No. 4 (1994) The CCP4 suite: programs for protein crystallography, *Acta Crystallogr., Sect. D 50*, 760−763.
25. Brunger, A. T., Adams, P. D., Clore, G. M., DeLano, W. L., Gros, P., Grosse, K. R. W., Jiang, J. S., Kuszewski, J., Nilges, M., Pannu, N. S., Read, R. J., Rice, L. M., Simonson, T., and Warren, G. L. (1998) Crystallography & NMR system: a new software suite for macromolecular structure determination, *Acta Crystallogr., Sect. D 54*, 905−921.
26. Roussel, A., Inisan, A. G., Knoop-Mouthuy, A., and Cambillau, C. (1999) Turbo-Frodo, Version OpenGL:1, CNRS/Universitite, Marseille, Marseille, France.
27. Li, L., and Singh, B. (2000) Role of zinc binding in type A botulinum neurotoxin light chain's toxic structure, *Biochemistry 39*, 10581−10586.
28. Simpson, L. L., Maksymowych, A. B., and Hao, S. (2001) The role of zinc binding in the biological activity of botulinum toxin, *J. Biol. Chem. 276*, 27034−27041.
29. Holmes, M. A., and Matthews, B. W. (1981) Binding of hydroxamic acid inhibitors to crystalline thermolysin suggests a pentacoordinate zinc intermediate in catalysis, *Biochemistry 20*, 6912−6920.
30. Boldt, G. E., Kennedy, J. P., Hixon, M. S., McAllister, L. A., Barbieri, J. T., Tzipori, S. T., and Janda, K. D. (2006) Synthesis, characterization and development of a high-throughput methodology for the discovery of botulinum nerotoxin A inhibitors, *J. Comb. Chem.*, published online May 19, http://dx.doi.org/10.1021/cc060010h.
31. Clayton, M. A., Clayton, J. M., Brown, D. R., and Middlebrook, J. L. (1995) Protective vaccination with a recombinant fragment of *Clostridium botulinum* neurotoxin serotype A expressed from a synthetic gene in *Escherichia coli*, *Infect. Immun. 63*, 2738−2742.
32. Robinson, R. F., and Nahata, M. C. (2003) Management of botulism, *Ann. Pharmacother. 37*, 127−131.
33. Potter, K. J., Zhang, W., Smith, L. A., and Meagher, M. M. (2000) Production and purification of the heavy chain fragment C of botulinum neurotoxin, serotype A, expressed in the methylotrophic yeast *Pichia pastoris*, *Protein Expression Purif. 19*, 393−402.
34. Baldwin, M. R., Tepp, W. H., Pier, C. L., Bradshaw, M., Ho, M., Wilson, B. A., Fritz, R. B., Johnson, E. A., and Barbieri, J. T. (2005) Characterization of the antibody response to the receptor binding domain of botulinum neurotoxin serotypes A and E, *Infect. Immun. 73*, 6998−7005.
35. Wu, H. C., Yeh, C. T., Huang, Y. L., Tarn, L. J., and Lung, C. C. (2001) Characterization of neutralizing antibodies and identification of neutralizing epitope mimics on the *Clostridium botulinum* neurotoxin type A, *Appl. Environ. Microbiol. 67*, 3201−3207.
36. Holmes, M. A., and Matthews, B. W. (1982) Structure of thermolysin refined at 1.6 Å resolution, *J. Mol. Biol. 160*, 623−639.
37. Schmidt, J. J., and Stafford, R. G. (2003) Fluorigenic substrates for the protease activities of botulinum neurotoxins, serotypes A, B, and F, *Appl. Environ. Microbiol. 69*, 297−303.
38. Burnett, J. C., Schmidt, J. J., Stafford, R. G., Panchal, R. G., Nguyen, T. L., Hermone, A. R., Vennerstrom, J. L., McGrath, C. F., Lane, D. J., Sausville, E. A., Zaharevitz, D. W., Gussio, R., and Bavari, S. (2003) Novel small molecule inhibitors of botulinum neurotoxin A metalloprotease activity, *Biochem. Biophys. Res. Commun. 310*, 84−93.
39. Park, J. G., Sill, P. C., Makiyi, E. F., Garcia-Sosa, A. T., Millard, C. B., Schmidt, J. J., and Pang, Y. P. (2006) Serotype-selective, small-molecule inhibitors of the zinc endopeptidase of botulinum neurotoxin serotype A, *Bioorg. Med. Chem. 14*, 395−408.
40. Ascher, B., and Rossi, B. (2004) Botulinum toxin and wrinkles: few side effects and effective combining procedures with other treatments, *Ann. Chir. Plast. Esthet. 49*, 537−552.
41. Klein, A. W. (2004) Complications with the use of botulinum toxin, *Dermatol. Clin. 22*, 197−205.
42. Bhidayasiri, R., and Truong, D. D. (2005) Expanding use of botulinum toxin, *J. Neurol. Sci. 235*, 1−9.
43. Mandal, A., and Robinson, R. J. (2001) Indications and efficacy of botulinum toxin in disorders of the gastrointestinal tract, *Eur. J. Gastroenterol. Hepatol. 13*, 603−609.
44. Kraulis, J. (1991) MOLSCRIPT: a program to produce both detailed and schematic plots of protein structures, *J. Appl. Crystallogr. 24*, 946−950.
45. Merritt, E. A., and Murphy, M. E. P. (1994) Raster3D, *Acta Crystallogr., Sect. D 50*, 869−873.

BI060786Z